ORIGINAL ARTICLE

JBMR®

Pulsed Electromagnetic Fields Partially Preserve Bone Mass, Microarchitecture, and Strength by Promoting Bone Formation in Hindlimb-Suspended Rats

Da Jing,[1] Jing Cai,[2]* Yan Wu,[3]* Guanghao Shen,[1] Feijiang Li,[1] Qiaoling Xu,[4] Kangning Xie,[1] Chi Tang,[1] Juan Liu,[1] Wei Guo,[1] Xiaoming Wu,[1] Maogang Jiang,[1] and Erping Luo[1]

[1]Department of Biomedical Engineering, Fourth Military Medical University, Xi'an, China
[2]Department of Endocrinology, Xijing Hospital, Fourth Military Medical University, Xi'an, China
[3]Institute of Orthopaedics, Xijing Hospital, Fourth Military Medical University, Xi'an, China
[4]Department of Nursing, Fourth Military Medical University, Xi'an, China

ABSTRACT

A large body of evidence indicates that pulsed electromagnetic fields (PEMF), as a safe and noninvasive method, could promote in vivo and in vitro osteogenesis. Thus far, the effects and underlying mechanisms of PEMF on disuse osteopenia and/or osteoporosis remain poorly understood. Herein, the efficiency of PEMF on osteoporotic bone microarchitecture, bone strength, and bone metabolism, together with its associated signaling pathway mechanism, was systematically investigated in hindlimb-unloaded (HU) rats. Thirty young mature (3-month-old), male Sprague-Dawley rats were equally assigned to control, HU, and HU + PEMF groups. The HU + PEMF group was subjected to daily 2-hour PEMF exposure at 15 Hz, 2.4 mT. After 4 weeks, micro–computed tomography (μCT) results showed that PEMF ameliorated the deterioration of trabecular and cortical bone microarchitecture. Three-point bending test showed that PEMF mitigated HU-induced reduction in femoral mechanical properties, including maximum load, stiffness, and elastic modulus. Moreover, PEMF increased serum bone formation markers, including osteocalcin (OC) and N-terminal propeptide of type 1 procollagen (P1NP); nevertheless, PEMF exerted minor inhibitory effects on bone resorption markers, including C-terminal crosslinked telopeptides of type I collagen (CTX-I) and tartrate-resistant acid phosphatase 5b (TRAcP5b). Bone histomorphometric analysis demonstrated that PEMF increased mineral apposition rate, bone formation rate, and osteoblast numbers in cancellous bone, but PEMF caused no obvious changes on osteoclast numbers. Real-time PCR showed that PEMF promoted tibial gene expressions of Wnt1, LRP5, β-catenin, OPG, and OC, but did not alter RANKL, RANK, or Sost mRNA levels. Moreover, the inhibitory effects of PEMF on disuse-induced osteopenia were further confirmed in 8-month-old mature adult HU rats. Together, these results demonstrate that PEMF alleviated disuse-induced bone loss by promoting skeletal anabolic activities, and imply that PEMF might become a potential biophysical treatment modality for disuse osteoporosis. © 2014 American Society for Bone and Mineral Research.

KEY WORDS: PULSED ELECTROMAGNETIC FIELDS; DISUSE; HINDLIMB UNLOADING; THREE-POINT BENDING TEST; BONE TURNOVER; WNT/LRP5/β-CATENIN SIGNALING

Introduction

Disuse osteoporosis is a common skeletal disease caused by the removal of weight-bearing physical activities, and characteristically occurs in patients with prolonged therapeutic bed rest and limb immobilization (eg, spinal cord injury and fracture), and in populations with long-duration exposure to microgravity environment (eg, astronauts).[1,2] Profound loss of bone mineral density (BMD) with approximately 1.5% per month occurs in astronauts during spaceflight, equaling that in postmenopausal women in 1 year.[3–5] Studies also showed that crewmembers during spaceflight experienced reduced bone formation, augmented bone resorption, and persistently higher fracture risk even 1 year after returning to Earth.[6,7] Similarly, mechanical unloading also led to significant BMD decrease and concomitant higher incidence of bone fractures for patients with long-term bed rest or immobilization.[8,9] In view of the side effects or high cost of antiosteoporosis drugs (eg, calcitonin, hormones, and calcium and vitamin D preparations),[10–14] safe and noninvasive biophysical countermeasures for disuse osteoporosis might be more promising in clinical application, and especially favorable for the use of spaceflight.

Our growing understanding of the intricate piezoelectric properties of bone tissues raised the possibility that exogenous

Received in original form November 10, 2013; revised form March 9, 2014; accepted March 31, 2014. Accepted manuscript online April 18, 2014.
Address correspondence to: Erping Luo, PhD, Department of Biomedical Engineering, Fourth Military Medical University, 17 West Changle Road, Xi'an 710032, China. E-mail: erpingluo@hotmail.com
*DJ, JC, and YW contributed equally to this work.
Additional Supporting Information may be found in the online version of this article.
Journal of Bone and Mineral Research, Vol. 29, No. 10, October 2014, pp 2250–2261
DOI: 10.1002/jbmr.2260
© 2014 American Society for Bone and Mineral Research

electric or magnetic stimulation might regulate the activities and functions of bone cells. Subsequent studies have confirmed the osteogenic effects of electrical stimulation.[15,16] Since the 1970s when Bassett and colleagues[17] for the first time found that pulsed electromagnetic field (PEMF) treatment, a more accessible and affordable noncontact modality, was able to accelerate fracture healing in patients, abundant evidence has substantiated that PEMF exposure is capable of producing satisfying therapeutic effects on a wide range of bone diseases, such as fresh and nonunion fractures[18,19] and osteoarthritis.[20,21] It has been suggested that the positive effects derived from PEMF might be primarily because induction of pulsed electric currents in bones initiates a battery of biological cascades.[22] Moreover, growing evidence has also shown the potential of PEMF in the treatment of osteopenia and/or osteoporosis. It has been proved that PEMF stimulation is capable of preventing the loss of bone mass and improving bone's biomechanical properties in osteoporotic rats induced by ovariectomy (OVX) or diabetes mellitus.[23–26] The antiosteoporosis efficiency of PEMF was further confirmed by several clinical investigations.[27–29] A large body of in vitro evidence has demonstrated that PEMF stimulation was able to promote proliferation and mineralization of osteoblasts[30–32] and also inhibit osteoclastogenesis.[33,34] Despite these positive findings, little is known about the mechanisms of PEMF exposure in relation to disuse-induced osteopenia and/or osteoporosis.

The tail-suspended hindlimb-unloaded (HU) rat model has been widely accepted as an effective animal model for simulating weightlessness and investigating disuse osteoporosis.[35] Rats subjected to HU displayed decreased bone formation and increased bone resorption, and thus led to concomitant loss of bone mass and reduction of bone mechanical strength.[36,37] Therefore, in the present investigation, we hypothesize that PEMF might regulate bone remodeling in HU rats, and subsequently inhibit disuse-induced deterioration of bone microarchitecture and decrease of bone mechanical strength. The effects of PEMF exposure on disuse-induced bone loss were evaluated via systematic analysis for serum biochemical, bone biomechanical, micro–computed tomography (μCT), and histomorphometric parameters in rats subjected to tail suspension. Moreover, the molecular signaling pathway mechanisms of PEMF on bone metabolism in HU rats, including osteoblastogenesis-related Wnt/LRP5/β-catenin signaling and osteoclastogenesis-associated RANKL-RANK signaling were preliminarily investigated.

Materials and Methods

Experimental design and animal model

All procedures in the experiment were approved by the Institutional Animal Care and Use Committee of the Fourth Military Medical University. Thirty young mature 3-month-old male Sprague-Dawley rats (276.0 ± 11.3 g; Vital River Laboratory Animal Technology, Beijing, China) were used in this study. Rats were divided into three equal groups ($n = 10$) and randomly assigned to the control, HU, and HU with PEMF exposure (HU + PEMF) groups. HU by the tail-suspension technique was employed according to a previously described protocol.[38] Briefly, the tail, after being cleaned with 70% ethanol, was coated with a thin layer of liquid-like benzoin and resin dissolved in 99% ethanol. A strip of adhesive tape was then firmly attached laterally along the proximal portion of the tail and allowed to thoroughly air dry, forming a loop close to the end of the tail. The adhesive tape was subsequently secured by three tape strips in its perpendicular direction. A plastic paperclip was employed to attach the loop of the surgical tape to a swivel hoop mounted at the top of a custom-designed Plexiglas cage (length = 35 cm, width = 30 cm, height = 45 cm). The rat was maintained in an approximately 30-degree head-down-tilt position with its hindlimbs unloaded. Rats were caged individually and allowed free access to tap water and chow. Rats in the HU + PEMF group were subjected to 2 hours/d whole-body PEMF exposure for 4 weeks. All animals received intramuscular injections of 25 mg/kg tetracycline (Sigma-Aldrich, St. Louis, MO, USA) 14 and 13 days before euthanasia, and 5 mg/kg calcein (Sigma-Aldrich) 4 and 3 days before euthanasia, respectively. At the end of the 4-week experiment, rats were euthanatized with an overdose of chloral hydrate. Serum samples were obtained via abdominal aorta puncture, centrifuged for 20 minutes and stored at −70°C for biochemical analysis. Bilateral femurs were harvested, wrapped in saline-soaked gauze, and stored at −70°C. Left femurs were used for mechanical testing, and right femurs were employed for μCT and histology analysis. Left tibias were harvested and stored in liquid nitrogen for real-time PCR and right tibias were used for bone histomorphometric analysis.

PEMF exposure

As described in our previous studies,[24,25,39] the PEMF waveform used in the experiment consisted of a pulsed burst (burst width, 5 ms; pulse width, 0.2 ms; pulse wait, 0.02 ms; burst wait, 60 ms; pulse rise, 0.3 μs; pulse fall, 2.0 μs) repeated at 15 Hz (Fig. 1). In brief, the PEMF exposure system was composed of a signal generator and a Helmholtz coil assembly with three-coil array (Fig. 1). The three coils were placed coaxially 304 mm apart from each other, and the number of turns of the central coil and outside coils were 266 turns and 500 turns, respectively. This assembly of three coils has exhibited significantly higher magnetic field uniformity.[25] To calculate the current in the coils, a resistor of 2 Ω was placed in series with the coils, and the voltage drop across the resistor was observed with an oscilloscope (Agilent Technologies, Santa Clara, CA, USA). The waveform and amplitude of the magnetic field produced by the PEMF generator were monitored with the oscilloscope all the time during the PEMF exposure. The peak magnetic field of the coils was determined to be 2.39 ± 0.03 mT. The peak magnetic field exhibited <0.01 mT fluctuation during daily 2-hour PEMF treatment, and displayed <0.02 mT variation on different days of measurements. The accuracy for the peak magnetic field measurement was further confirmed by using a Gaussmeter (Model 455 DMP Gaussmeter; Lake Shore Cryotronics, Westerville, OH, USA). The measured background electromagnetic field was 0.05 ± 0.002 mT.

Serum biochemical analysis

Serum markers for bone formation including serum osteocalcin (OC) and N-terminal propeptide of type 1 procollagen (P1NP), and bone resorption markers including serum tartrate-resistant acid phosphatase 5b (TRAcP5b) and C-terminal cross-linked telopeptides of type I collagen (CTX-I) in the rats of the three groups ($n = 10$) were quantified with commercial ELISA kits (Biomedical Technologies, Stoughton, MA, USA). Assays were performed according to the protocols provided by the manufacturers.

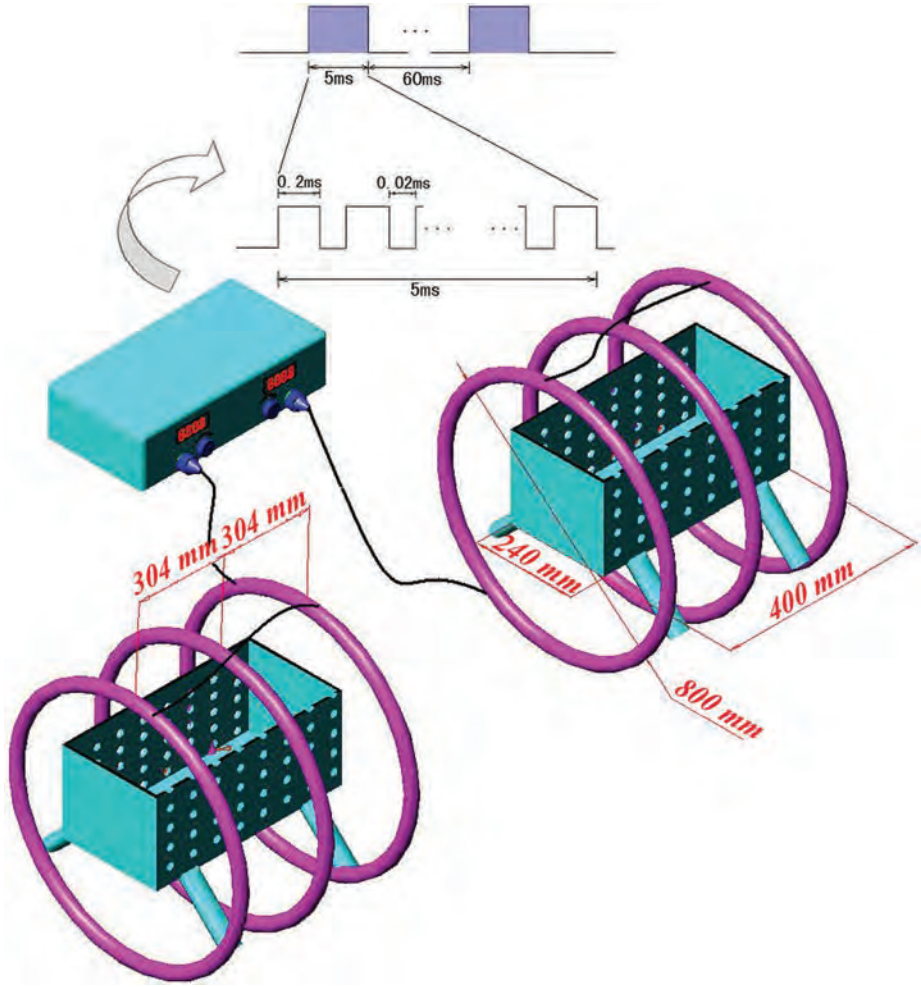


Fig. 1. Schematic representation of the PEMF generator together with a Helmholtz coil assembly with three-coil array.[21] The PEMF output waveform consisted of a pulsed burst (burst width, 5 ms; pulse width, 0.2 ms; pulse wait, 0.02 ms; burst wait, 60 ms; pulse rise, 0.3 μs; pulse fall, 2.0 μs) repeated at 15 Hz. The peak magnetic field within the Helmholtz coils was 2.39 ± 0.03 mT. PEMF = pulsed electromagnetic field.

Biomechanical examination

The left femurs of the rats ($n = 10$ for each group) were subjected to three-point bending test to evaluate the biomechanical properties using a commercial mechanical testing device (AGS-10kNG; Shimadzu, Kyoto, Japan). The femur, with its physiological curvature facing up, was stabilized on a supporter with two fixed loading points with 20-mm distance. The upper loading plate was oriented perpendicularly to the long axis of the sample. A preload with 2 N was applied to immobilize the sample prior to mechanical testing. Then, load was applied at a constant displacement rate of 2 mm/min by controlling the motion of the upper loading plate until fracture occurred. Then, the lengths of the internal and external major axis and minor axis of the femur at the fracture point were immediately measured using a vernier caliper. The parameters of structural properties were calculated from the load-displacement curve, including maximum load, yield load, ultimate displacement, yield displacement, stiffness, and energy absorption. The parameters of bulk material properties were calculated from the stress-strain curve that was normalized by the geometrical measurements, including maximum stress, yield stress, ultimate strain, yield strain, and toughness.[40]

μCT analysis

The bone microarchitecture of right femurs of the rats ($n = 10$ for each group) was evaluated using a high-resolution μCT (GE Healthcare, Madison, WI, USA) with a scanning resolution of 16 μm/slice. Bone samples were placed in a 20-mm-diameter sample tube perpendicularly to the scanning axis with a total 20-mm reconstruction height. The basic parameters of the scanner were the following: voltage 80 kV, current 80 μA, exposure time 2.96 seconds, total rotation angle 210 degrees, and rotation angle of increment 0.4 degrees. After scanning, 2D image sequences were transferred to a workstation and 3D images were reconstructed. A volume of interest (VOI) with 2.0-mm height was selected for the analysis of trabecular bone microarchitecture. The VOI started at a distance of 0.4 mm from the lowest end of the growth plate of the distal femur and

extended to the proximal end with a distance of 2.0 mm, which excluded all the primary spongiosa and only contained the second spongiosa. All 3D manipulations and analyses were performed using the MicroView program (GE Healthcare). The trabecular bone parameters, including trabecular BMD, trabecular number (Tb.N), trabecular thickness (Tb.Th), trabecular separation (Tb.Sp), bone volume per tissue volume (BV/TV), structure model index (SMI), connectivity density (Conn.D), and bone surface per bone volume (BS/BV) were quantified. The mid-diaphyseal cortical thickness (Ct.Th), cortical area (Ct.Ar), total cross-sectional area inside the periosteal envelope (Tt.Ar), and cortical bone fraction (Ct.Ar/Tt.Ar) were also determined.[41]

Histology and histomorphometry of trabecular bone

After μCT scanning, samples were stained with Van Gieson to further evaluate the cancellous bone histology. Right tibias were cut longitudinally into two pieces along the sagittal plane after animal dissection. One piece was fixed in 4% paraformaldehyde (PFA), decalcified in 10% ethylenediaminetetraacetic acid (EDTA), and then embedded in paraffin. Sections with 5 μm thick were stained with toluidine blue to visualize osteoblasts, and stained with hematoxylin and eosin (H&E) to label osteoclasts. Static trabecular bone histomorphometric parameters, including osteoblast numbers per millimeter of trabecular bone surface (N.Ob/BS) and osteoclast numbers per millimeter of trabecular bone surface (N.Oc/BS) were quantified ($n = 10$ for each group). The other piece was fixed in 80% ethanol for 24 hours, and then embedded in methylmethacrylate. Unstained Sections with 80 μm thick were imaged using fluorescence microscope (LEICA DM LA; Leica Microsystems, Heidelberg, Germany) to quantify the dynamic trabecular bone histomorphometric parameters ($n = 10$ for each group), including mineral apposition rate (MAR), mineralizing surface per bone surface (MS/BS), and bone formation rate per bone surface (BFR/BS). For histomorphometric analysis, one section was measured for each sample, and all sections were coded and analyzed "blind" by one independent observer. The region that was 0.5 mm to 2 mm higher than the highest end of the growth plate of the proximal tibia was defined as the VOI for histomorphometric analysis, which only contained the secondary spongiosa. Two repeated measurements were performed for each section within the selected VOI.

Real-time PCR

After animal scarification, soft tissues and muscles from left tibial bone samples ($n = 10$ for each group) were immediately removed on ice. The mid-diaphysis of the tibia with 1.5-cm length was spun at 4472 g for 3 minutes in the centrifuge to remove the bone marrow. Bone samples were then snap-frozen in liquid nitrogen. Before RNA extraction, samples were immediately crushed into powder in a mortar containing liquid nitrogen using a pestle and then mixed with a monophasic solution of phenol and guanidine thiocyanate. Total RNA was extracted using the guanidinium isothiocyanate-alcohol phenyl-chloroform method according to the manufacturer's instructions. Then, SuperScript III reverse transcriptase was used to synthesize cDNA from RNA. Real-time fluorescence quantitative polymerase chain reaction (PCR) was performed on ABI 7300 Real-Time PCR system using the SYBR Green PCR Master Mix (Applied Biosystems, Foster City, CA, USA). The primers were synthesized by Nanjing Genscript Biological Engineering Technology & Service Co., Ltd. (Nanjing, China). The primers used in this study are shown in Table 1. All mRNA levels were normalized by the housekeeping gene glyceraldehyde 3-phosphate dehydrogenase (GAPDH).

Statistical analysis

All data in this study were expressed as the mean ± SD. Statistical analyses were performed using Microsoft SPSS 13.0 software (SPSS, Chicago, IL, USA). All data presented in this study were examined for normal distribution using the Kolmogorov-Smirnov test, and evaluated for homogeneity of variance using the Levene test. Analyses showed that each specific parameter in the three groups obeyed normal distribution and homoscedasticity. One-way analysis of variance (ANOVA) was used for evaluating the existence of differences among the three groups, and once a significant difference was detected, Bonferroni's post hoc analysis was used to determine the significance between every two groups. Values of $p < 0.05$ were considered statistically significant.

Table 1. The Sequence of Primers Used in the Present Study for Real-Time Fluorescence Quantitative PCR

Genes	Primers	Primer Sequence (5′-3′)	Product Length (bp)
Osteocalcin	Forward	GGGCAGTAAGGTGGTGAATAG	241
	Reverse	AGTCCTGGAGAGTAGCCAAAG	
Wnt1	Forward	CGAGGTGAAAGGGCAAGGAAAG	165
	Reverse	TGATGAAGAGGGAGCAGGACAG	
LRP5	Forward	TGCCACTGGTGAGATTGAC	221
	Reverse	ACTGCTGCTTGATGAGGAC	
β-catenin	Forward	TCACGCAAGAGCAAGTAG	149
	Reverse	CTGGACATTAGTGGGATGAG	
OPG	Forward	CTGGGCTGTTTCTTCAGGATG	224
	Reverse	CTCTTTCTCAGGGTGCTTGAC	
RANKL	Forward	AGCGAAGACACAGAAGCACTAC	228
	Reverse	TTTATGGGAACCCGATGGGATG	
RANK	Forward	TATTTGGCACTCCTCTCAC	158
	Reverse	TGTCCCTTTCACTCTTTGG	
Sost	Forward	TGATGCCACAGAAATCATCC	132
	Reverse	ACGTCTTTGGTGTCATAAGG	

Table 2. Comparisons of Body Weights of Young Mature Rats in the Three Experimental Groups Before and After PEMF Exposure

Body weight (g)	Control	HU	HU + PEMF
Day 0	275.6 ± 12.9	275.6 ± 12.6	277.2 ± 9.7
Day 29	354.3 ± 20.9	293.6 ± 16.7*	295.0 ± 24.8*
Body weight change (g)	78.6 ± 14.5	18.0 ± 12.5*	18.1 ± 15.8*

Values are expressed as mean ± S.D. ($n = 10$).
HU = hindlimb-unloaded; PEMF = pulsed electromagnetic field.
*Significant difference from the Control group with $P < 0.05$.

Results

Body weight measurement

As shown in Table 2, body weights of rats in the three groups before the experiment had no significant difference. After 4-week tail suspension, body weights of rats in the HU group and HU + PEMF group were significantly lower than those in the control group ($p < 0.01$). However, no obvious difference in body weights was observed between the HU group and HU + PEMF group ($p = 0.999$).

Serum biochemical examination

As shown in Fig. 2, HU resulted in significant decrease in serum OC and P1NP (bone formation markers) ($p < 0.01$), and increase in serum CTX-I and TRAcP5b (bone resorption markers) ($p < 0.01$). In comparison with the HU group, 4-week PEMF exposure significantly increased the secretions of serum OC and P1NP ($p < 0.05$, +47.0% and +59.2%, respectively), and also caused minor decrease in the levels of serum CTX-I and TRAcP5b ($p < 0.05$ for CTX-I and $p = 0.121$ for TRAcP5b, −16.4% and −15.2%, respectively). No significant difference was found in OC, P1NP, CTX-I, or TRAcP5b between the control and HU + PEMF groups ($p = 0.495$, 0.155, 0.177, and 0.147, respectively).

Biomechanical testing

The results of femoral structural properties and bulk material properties via three-point bending test are shown in Fig. 3 and Supporting Fig. S1, respectively. The structural parameters of the rat femurs, including maximum load, yield load, ultimate displacement, yield displacement, stiffness, and energy absorption, and bulk material properties, including maximum stress,

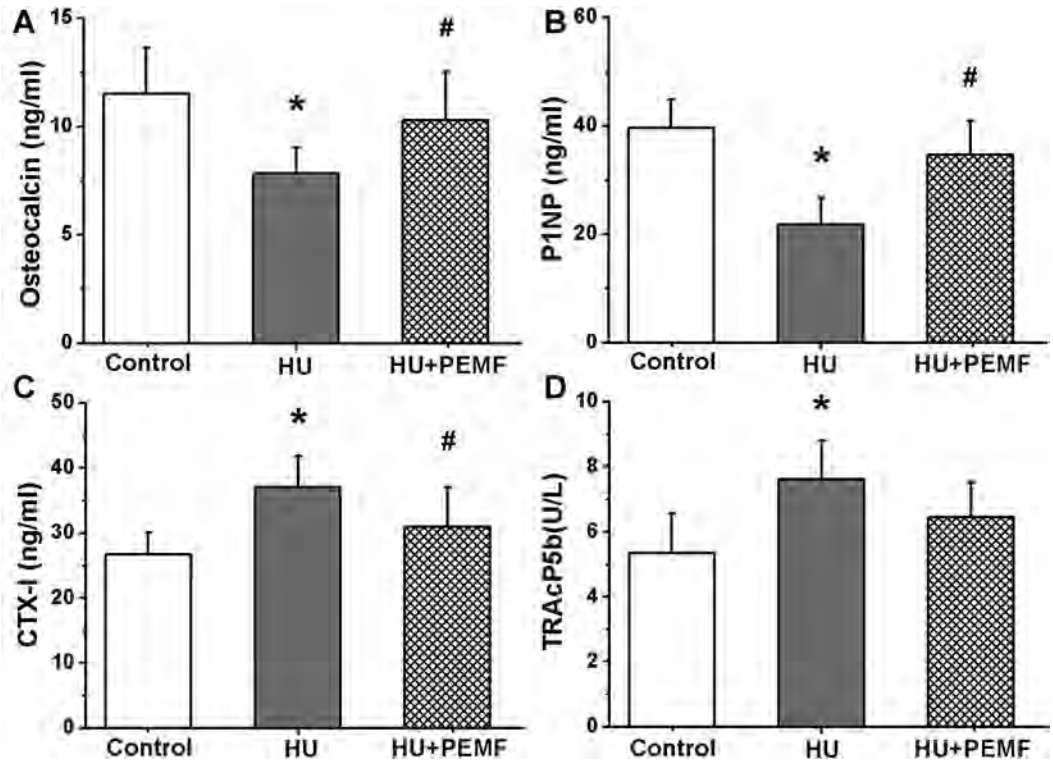


Fig. 2. Effects of 4-week PEMF exposure on serum biochemical indices (bone turnover markers) in HU rats, including bone formation markers (*A*) OC and (*B*) P1NP, and bone resorption markers (*C*) CTX-I and (*D*) TRAcP5b. Values are all expressed as mean ± SD ($n = 10$). *Significant difference from the control group with $p < 0.05$. #Significant difference from the HU group with $p < 0.05$. PEMF = pulsed electromagnetic field; HU = hindlimb-unloaded; HU + PEMF, hindlimb unloading with PEMF exposure; OC = osteocalcin; P1NP = N-terminal propeptide of type 1 procollagen; CTX-I = C-terminal cross-linked telopeptides of type I collagen; TRAcP5b = tartrate-resistant acid phosphatase 5b.

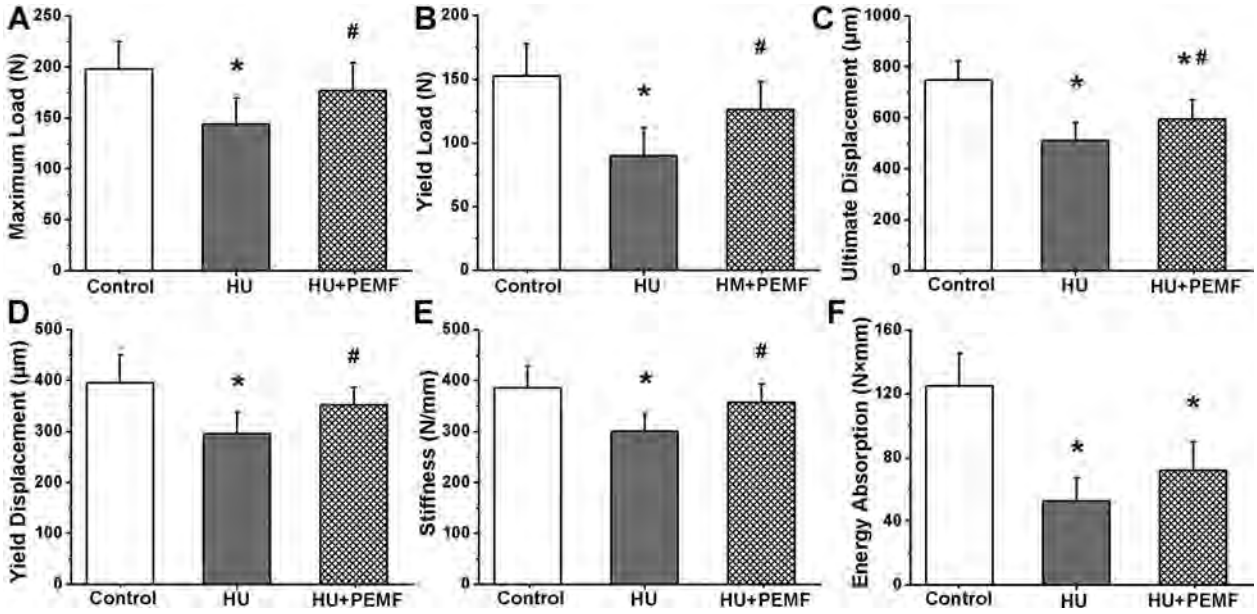


Fig. 3. Effects of 4-week PEMF exposure on femoral biomechanical structural properties in HU rats via three-point bending test, including maximum load (*A*), yield load (*B*), ultimate displacement (*C*), yield displacement (*D*), stiffness (*E*), and energy absorption (*F*). Values are all expressed as mean ± SD ($n = 10$). *Significant difference from the control group with $p < 0.05$. #Significant difference from the HU group with $p < 0.05$. PEMF = pulsed electromagnetic field; HU = hindlimb-unloaded; HU + PEMF = hindlimb unloading with PEMF exposure.

yield stress, ultimate strain, and toughness in the HU group were significantly lower than those in the control group ($p < 0.05$). PEMF significantly increased maximum load, yield load, ultimate displacement, yield displacement, stiffness, maximum stress, yield stress, and toughness of the femurs in HU rats ($p < 0.05$, +22.7%, +40.0%, +16.9%, +18.6%, +18.9%, +21.3%, +38.8%, and +20.2%, respectively). PEMF stimulation did not exhibit statistically significant increase in femoral energy absorption ($p = 0.273$) or ultimate strain ($p = 0.128$) in HU rats. Moreover, ultimate displacement, energy absorption, maximum stress, yield stress, ultimate strain, yield strain, and toughness in the control group were significantly higher than those in the HU + PEMF group ($p < 0.05$); nevertheless, no significant difference was observed in femoral maximum load, yield load, yield displacement, or stiffness between the control group and HU + PEMF group ($p = 0.254$, 0.052, 0.119, and 0.315, respectively).

μCT analysis

Representative μCT images for trabecular and cortical bone microarchitecture in the three experimental groups are shown in Fig. 4*A–C*. The femurs from HU rats displayed notable reduction in the trabecular number, trabecular connection, trabecular area, and cortical thickness compared with those in the control group. PEMF partially inhibited disuse-induced deterioration of trabecular bone microarchitecture and decrease of cortical bone thickness (Fig. 4*B*, *C*). As shown in Fig. 4*D–K*, HU resulted in significant decrease in trabecular BMD, Tb.N, Tb.Th, BV/TV, and Conn.D ($p < 0.01$), and increase in Tb.Sp, SMI, and BS/BV ($p < 0.01$). Moreover, HU caused significant decrease in the cortical bone parameters (Ct.Ar, Ct.Th, and Ct.Ar/Tr.Ar) as compared with the control group ($p < 0.01$), but did not exert significant change in Tr.Ar ($p = 0.999$; Fig. 4*L–O*). PEMF exposure significantly inhibited HU-induced reduction in trabecular BMD, Tb.N, BV/TV, and Conn.D ($p < 0.05$), and increase in Tb.Sp, SMI, and BS/BV ($p < 0.05$). PEMF also significantly increased Ct.Ar, Ct.Th, and Ct.Ar/Tr.Ar in HU rats ($p < 0.05$). Moreover, the control group exhibited higher Tb.N, BV/TV, Conn.D, Ct.Ar, and Ct.Th, and lower SMI than the HU + PEMF group ($p < 0.05$). No significant difference was observed in trabecular BMD, Tb.Th, Tb.Sp, BS/BV, or Ct.Ar/Tr.Ar between the control and HU + PEMF groups ($p = 0.180$, 0.100, 0.229, 0.433, and 0.262, respectively).

Histology and histomorphometry

As shown in Fig. 5A, 4-week PEMF exposure partially restored trabecular bone mass and bone microarchitecture in HU rats. Representative images of PEMF treatment on osteoblast and osteoclast formation on the surface of trabecular bone are shown in Fig. 5*B*, *C*. HU caused significantly increased osteoclast numbers and decreased osteoblast formation, whereas PEMF stimulation significantly promoted osteoblastogenesis and exerted only a minor inhibitory action on osteoclastogenesis. Statistical comparisons (Fig. 5*D–H*) demonstrate that HU resulted in significantly lower levels of N.Ob/BS, MAR, and BFR/BS, and higher levels of N.Oc/BS ($p < 0.01$). PEMF caused significantly higher N.Ob/BS ($p < 0.01$, +53.3%) and slightly lower N.Oc/BS ($p = 0.382$, −12.4%) compared with the HU group. Moreover, PEMF significantly increased MAR and BFR/BS as compared to the HU group ($p < 0.01$, +119.1% and +118.8%, respectively), whereas PEMF exerted no effects on MS/BS ($p = 0.997$). Furthermore, the control group exhibited higher N.Ob/BS, MAR, and BFR/BS, and lower N.Oc/BS ($p < 0.05$) than the HU + PEMF group, whereas no significant difference was found in MS/BS between the control and HU + PEMF groups

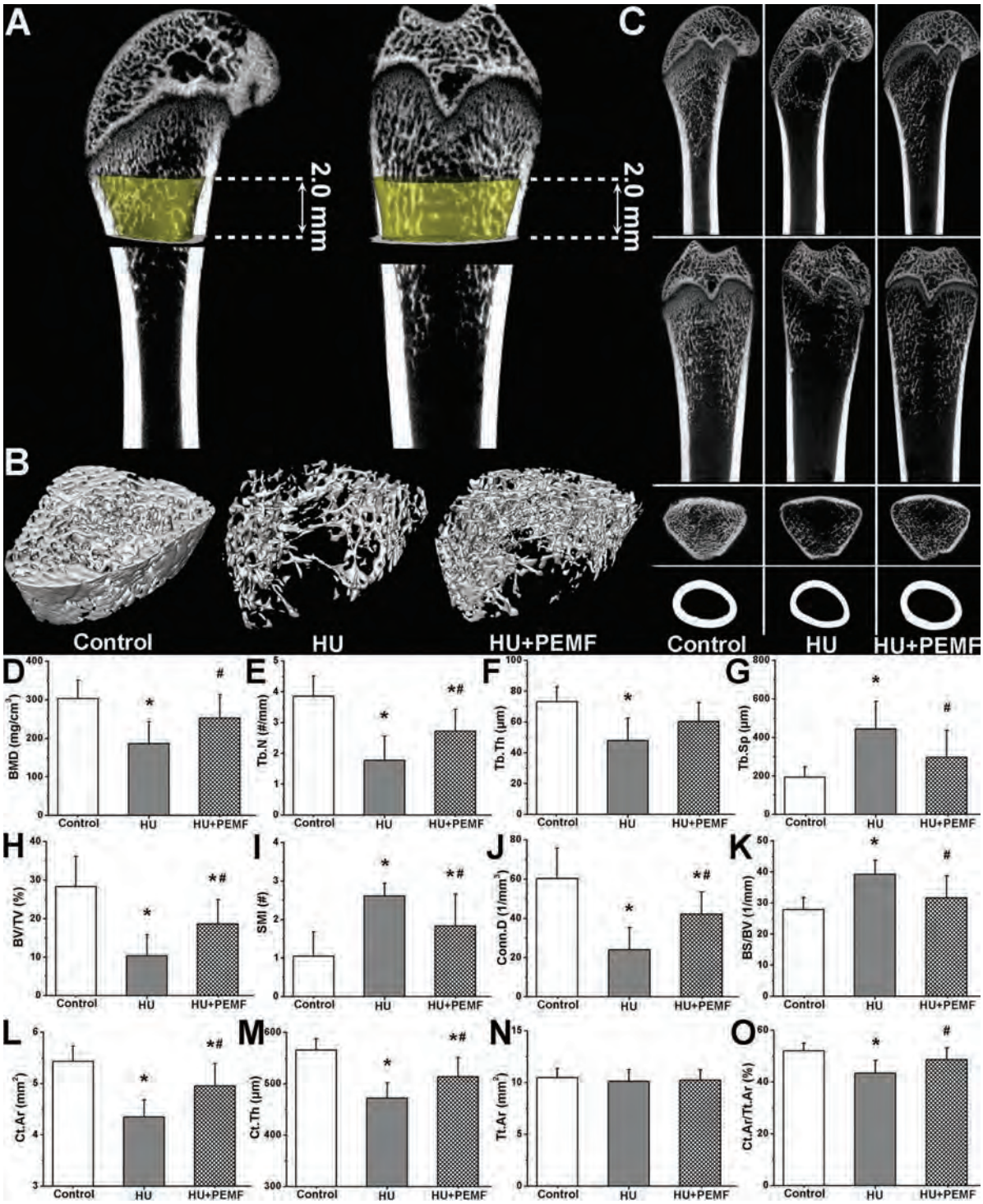


Fig. 4. Effects of 4-week PEMF exposure on trabecular bone microarchitecture in the distal femora and cortical bone thickness in the mid-diaphysis of the femurs. (*A*) The selected VOI with yellow color in 2.0 mm height, which only contains the secondary spongiosa. (*B*) 3D μCT images of trabecular bone microarchitecture determined by the VOI. (*C*) 2D μCT images of trabecular bone microarchitecture from the axial, coronal, and sagittal plane observation in the distal femora, and cortical bone structure in the mid-diaphysis of the femurs. Statistical comparisons of indices of trabecular bone microarchitecture, including trabecular (*D*) BMD, (*E*) Tb.N, (*F*) Tb.Th, (*G*) Tb.Sp, (*H*) BV/TV, (*I*) SMI, (*J*) Conn.D, and (*K*) BS/BV. Comparisons of indices of cortical bone structure, including (*L*) Ct.Ar, (*M*) Ct.Th, (*N*) Tt.Ar, and (*O*) Ct.Ar/Tt.Ar. Values are all expressed as mean ± SD ($n = 10$). *Significant difference from the control group with $p < 0.05$. #Significant difference from the HU group with $p < 0.05$. PEMF = pulsed electromagnetic field; VOI = volume of interest; BMD = bone mineral density; Tb.N = trabecular number; Tb.Th = trabecular thickness; Tb.Sp = trabecular separation; BV/TV = bone volume per tissue volume; SMI = structure model index; Conn.D = connectivity density; BS/BV = bone surface per bone volume; Ct.Ar = cortical area; Ct.Th = cortical thickness; Tt.Ar = total cross-sectional area; Ct.Ar/Tt.Ar = cortical bone fraction; HU = hindlimb-unloaded; HU + PEMF = hindlimb unloading with PEMF exposure.

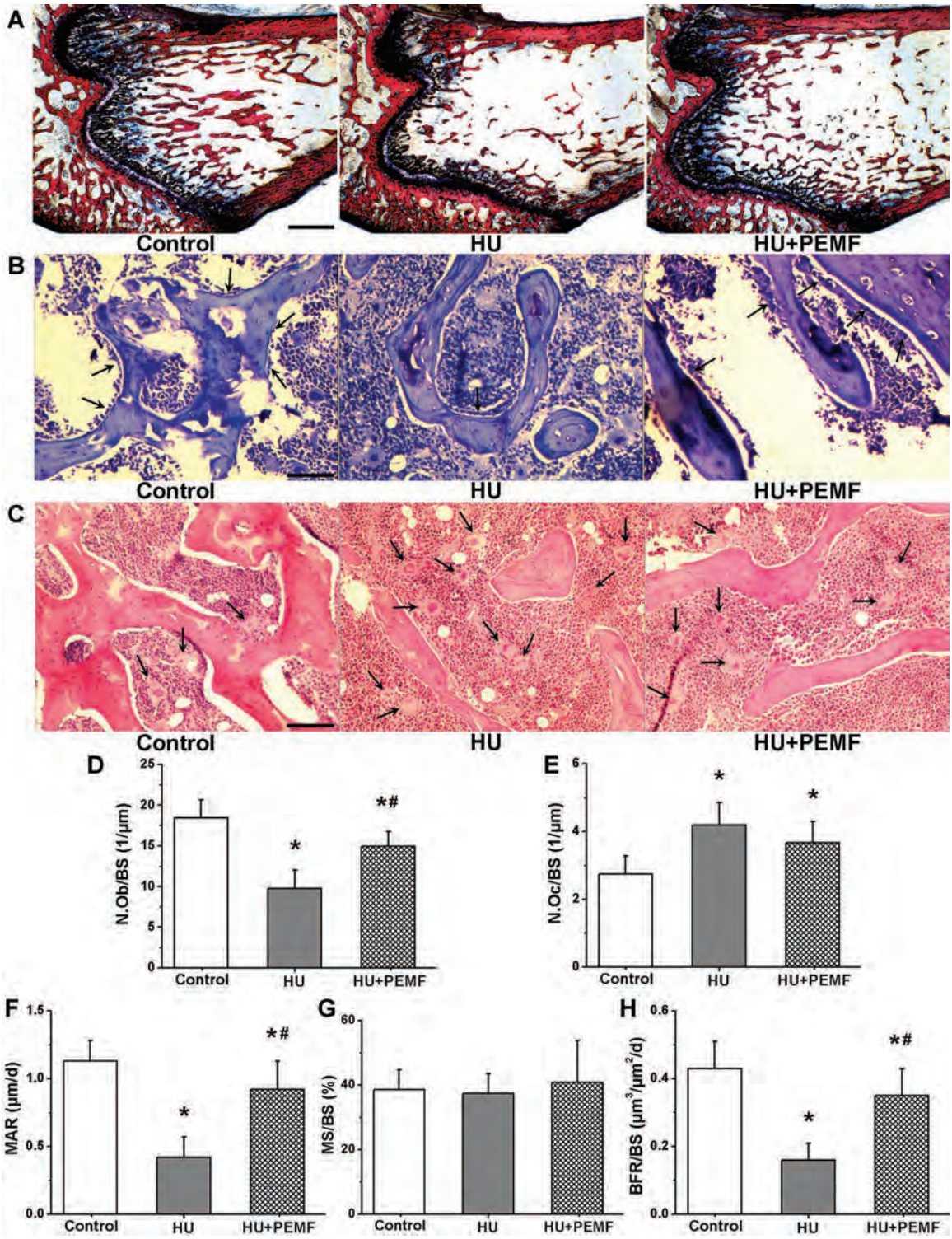


Fig. 5. Effects of 4-week PEMF exposure on trabecular bone histology and histomorphometry in HU rats. (*A*) Representative histological images for bone microarchitecture of the distal femora by Van Gieson staining. Scale bar = 1000 μm. Bone samples were stained with toluidine blue to visualize osteoblasts (*B*) and stained with hematoxylin and eosin to detect osteoclasts (*C*) in tibial trabecular bone. Arrows in *B* indicate osteoblasts, and arrows in *C* indicate osteoclasts. Scale bar = 300 μm in *B* and *C*. Comparisons of static histomorphometric parameters of trabecular bone, including (*D*) N.Ob/BS and (*E*) N.Oc/BS. Comparisons of dynamic histomorphometric parameters of trabecular bone by double labeling with tetracycline and calcein, including (*F*) MAR, (*G*) MS/BS, and (*H*) BFR/BS. Values are all expressed as mean ± SD ($n = 10$). *Significant difference from the control group with $p < 0.05$. #Significant difference from the HU group with $p < 0.05$. PEMF = pulsed electromagnetic field; HU = hindlimb-unloaded; HU + PEMF = hindlimb unloading with PEMF exposure; N.Ob/BS = number of osteoblasts per millimeter of trabecular bone surface; N.Oc/BS = number of osteoclasts per millimeter of trabecular bone surface; MAR = mineral apposition rate; MS/BS = mineralizing surface per bone surface; BFR/BS = bone formation rate per bone surface.

($p = 0.999$). The intraassay coefficients of variation for histomorphometric parameters were 3.3% (N.Ob/BS), 4.1% (N.Oc/BS), 3.8% (MAR), 4.3% (BFR/BS), and 4.2% (MS/BS).

Real-time PCR

The results of real-time PCR for Wnt1, LRP5, β-catenin, RANKL, RANK, OPG, OC, and Sost total mRNA expressions in tibial shaft are shown in Fig. 6. HU induced significant increase in Wnt1, LRP5, and β-catenin gene expressions in the canonical Wnt signaling ($p < 0.05$). PEMF significantly increased Wnt1, LRP5, and β-catenin mRNA levels in HU rats ($p < 0.01$). Moreover, no significant difference was observed in RANK or RANKL mRNA levels between the control, HU, and HU + PEMF groups. OPG and OPG/RANKL levels in the HU group were significantly lower than those in the control group ($p < 0.05$). PEMF caused significant increase in OPG mRNA expression ($p < 0.05$), whereas PEMF showed no significant increase in OPG/RANKL levels ($p = 0.225$). Furthermore, HU caused significant decrease in tibial bone formation marker OC and Sost mRNA expression that was exclusively secreted by osteocytes ($p < 0.05$). PEMF increased OC mRNA expression ($p < 0.01$), whereas PEMF showed no obvious effects on Sost mRNA expression ($p = 0.999$). Moreover, the control group showed lower Sost mRNA levels than the HU + PEMF group ($p < 0.05$). No significant difference in Wnt1, LRP5, β-catenin, RANK, RANKL, OPG, OPG/RANKL, or OC mRNA levels was observed between the control and HU + PEMF groups ($p = 0.181$, 0.267, 0.999, 1.000, 1.000, 0.326, 0.993, and 1.000, respectively).

Effects of PEMF on disuse-induced osteopenia in mature adult HU rats

μCT analysis showed no significant difference in trabecular BMD, BV/TV, and Tb.N after 2-day HU/PEMF stimulation between the control, HU, and HU + PEMF groups (Supporting Fig. S2A). Real-time PCR assays demonstrated that 2-day HU caused significant decrease in Wnt1 and LRP5 and increase in Sost mRNA levels ($p < 0.05$; Supporting Fig. S2B). Compared to the HU group, the HU + PEMF group exhibited higher Wnt1 and β-catenin mRNA levels ($p < 0.05$), whereas PEMF did not significantly change the LRP5, RANK, RANKL, or Sost gene expressions ($p = 0.127$, 1.000, 1.000, and 1.000, respectively). HU for 4 weeks resulted in significant decrease in bone microarchitecture, as evidenced by decreased trabecular BMD, BV/TV, and Tb.N ($p < 0.05$; Supporting Fig. S3A, B). PEMF exposure significantly increased trabecular

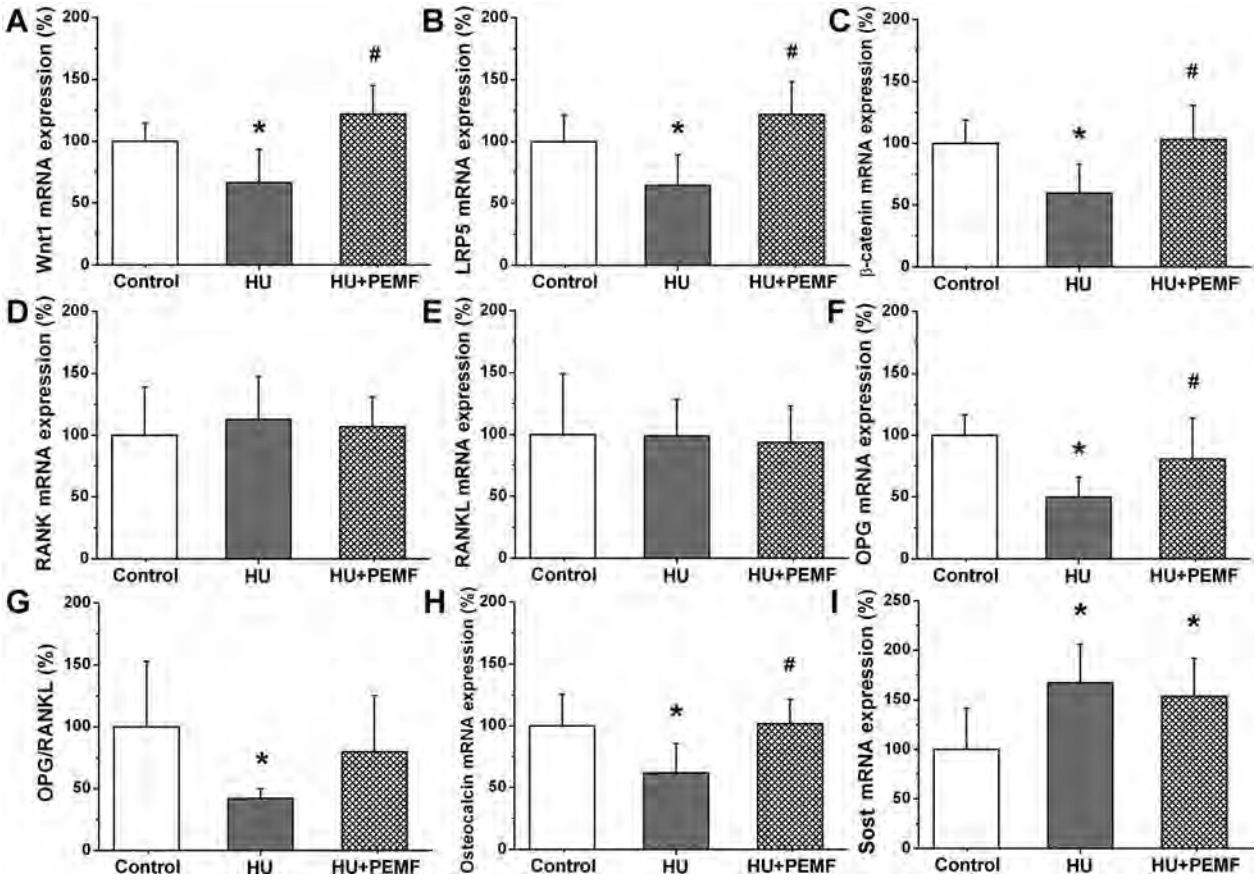


Fig. 6. Effects of 4-week PEMF exposure on gene expressions in the tibial shaft with the removal of bone marrow in HU rats by real-time fluorescence quantitative PCR analysis, including (*A*) Wnt1, (*B*) LRP5, (*C*) β-catenin, (*D*) RANKL, (*E*) RANK, (*F*) OPG, (*G*) OPG/RANKL, (*H*) osteocalcin, and (*I*) Sost mRNA expressions. Values are all expressed as mean ± SD ($n = 10$) and the relative expression level of each gene was normalized to GAPDH. *Significant difference from the control group with $p < 0.05$. #Significant difference from the HU group with $p < 0.05$. PEMF = pulsed electromagnetic field; HU = hindlimb-unloaded; HU + PEMF = hindlimb unloading with PEMF exposure.

BMD, BV/TV, and Tb.N in HU rats ($p < 0.05$). Moreover, HU caused significantly lower tibial Wnt1, LRP5, and β-catenin, and higher Sost mRNA levels ($p < 0.05$; Supporting Fig. S3C). PEMF promoted skeletal gene expressions of Wnt1, LRP5, and β-catenin ($p < 0.05$), but did not significantly change the RANK, RANKL, or Sost mRNA levels ($p = 1.000$ for all).

Discussion

PEMF have been proven to promote osteogenesis both experimentally and clinically[24,27]; nevertheless, no data to date have reported the effects of PEMF on unloading-induced bone loss together with their associated signaling pathway mechanisms. The present study demonstrates that PEMF exposure attenuated disuse-induced decrease of bone mass and deterioration of bone microarchitecture and mechanical strength in rats by promoting bone formation. The anabolic effects of PEMF might be associated with the increase of skeletal gene expressions of Wnt/Lrp5/β-catenin signaling. This study opens new alternatives for resisting unloading induced-bone loss in an easy and noninvasive manner.

Sharing similarities with humans who lose the normal weight-bearing activities (eg, spaceflight, long-term immobility, and bed rest), the rats with HU experience disturbed balance of bone metabolism, resulting in concomitant trabecular bone loss.[42,43] In line with previous findings,[42–44] our μCT observations revealed notable deterioration of trabecular bone microarchitecture in young mature 3-month-old rats, evidenced by decreased trabecular BMD, Tb.N, Tb.Th, BV/TV, and Conn.D, and increased Tb.Sp and BS/BV. HU also increased trabecular SMI, revealing an obvious reduction of plate-like structure.[45] Moreover, in accordance with several previous findings,[46,47] HU led to lower cortical bone thickness in 3-month-old rats, implying potential poorer capacity of fracture toughness. PEMF exposure for 4 weeks was able to significantly inhibit the deterioration of trabecular bone microarchitecture and decrease of cortical bone thickness, whereas both trabecular and cortical bone structure after PEMF treatment in HU rats could not be entirely restored to the normal condition. Moreover, our findings showed that 4-week PEMF exposure also attenuated the deterioration of bone microarchitecture in mature adult 8-month-old HU rats. Thus, our findings indicate that disuse-induced bone mass loss and deterioration of bone microarchitecture could be partially reversed by PEMF.

Consistent with previous findings,[47–49] the structural properties and bulk material properties were decreased in the femora of HU rats, revealing the impaired mechanical integrity and declining capacity of fracture resistance. However, the deterioration in extrinsic structural properties of bone, including maximum load, yield load, ultimate displacement, yield displacement, and stiffness was significantly inhibited by PEMF, implying increased mechanical strength of bone to resist fractures. Furthermore, PEMF exposure significantly increased the bulk material parameters of femurs (maximum stress, yield stress, and toughness) in HU rats, which reveals potential improvement in bone's intrinsic properties. Therefore, coupled with the μCT findings in cortical bone microarchitecture, our results indicate that PEMF stimulation was able to ameliorate the deterioration of both mechanical and structural properties of the cortical bone in HU rats, and thus improve bone's overall biomechanical performance. However, the limitation of whole-bone three-point bending test is that it cannot provide a precise measurement of the tissue-level elastic modulus,[50] which may need an independent study via systematic biomechanical examination using nanoindentation and ultrasound evaluation in the future work.

Bone maintains its normal structural and functional integrity via continuous remodeling activity, characterized by a dynamic balance between osteoblast-mediated bone formation and osteoclast-mediated bone resorption. Long-term skeletal unloading provides a perturbation in bone mineral homeostasis, resulting in decreased bone formation and increased bone resorption.[36,37] It is noted that serum OC and P1NP, as crucial bone formation markers, were significantly decreased in HU rats in this study, which was consistent with those by other investigators.[51,52] PEMF exposure significantly promoted serum OC and P1NP secretions as well as tibial overall OC mRNA expression, revealing obvious promotive effects of PEMF on osteoblastogenesis. Furthermore, 4-week HU led to significant increase in serum markers reflecting bone resorption, including TRAcP5b and CTX-I. Similar findings were also reported by several previous studies.[51,53] However, PEMF caused only modest inhibitory action on serum TRAcP5b and CTX-I. Thus, our results imply that the regulatory effects of PEMF on osteoclastogenesis were less prominent than those on osteoblastogenesis in HU rats. Moreover, the histomorphometric results further confirmed the modulating role of PEMF in bone remodeling with obvious anabolic and modest anti-resorptive effects. First, PEMF exposure significantly increased bone formation, as revealed by increased mineral apposition rate, bone formation rate, and osteoblast number. On the other hand, PEMF also exerted minor effects on osteoclast number. Together, our results suggest that the impacts of PEMF on disuse-induced bone loss in HU rats were largely associated with its promotion of bone formation.

Growing evidence has shown that osteoblastogenesis-associated canonical Wnt signaling and osteoclastogenesis-related RANKL-RANK signaling are critical for bone quality.[54–57] First, activation of canonical Wnt signaling increases bone formation via multiple routes, including promoting the differentiation of mesenchymal stem cells into mature osteoblasts, enhancing the proliferation and mineralization of osteoblasts, and preventing the osteoblast apoptosis.[55] Our findings demonstrate that 4-week PEMF exposure augmented the skeletal gene expressions in Wnt/Lrp5/β-catenin signaling in both young mature and mature adult HU rats, including Wnt1, LRP5, and β-catenin. Moreover, we also showed that the gene expressions in Wnt/Lrp5/β-catenin signaling were increased after 2-day PEMF stimulation when the bone structure is not significantly changed. Thus, our findings suggest that the anabolic effects of PEMF in HU rats might be associated with the increase of skeletal gene expressions of Wnt/Lrp5/β-catenin signaling. Second, the RANKL-RANK signaling acts as an essential pathway in osteoclast development and activation. RANKL is mainly secreted by osteoblasts and osteocytes in bone, and specifically binds with RANK located on the osteoclast cell membrane to trigger intricate signaling cascades.[56,57] Our findings showed that overall mRNA expression of either RANKL or RANK was not significantly altered in either young mature or mature adult HU rats after PEMF exposure, suggesting that RANKL-RANK signaling might play a minor role in the regulatory activity of PEMF in bone metabolism. Third, osteocytes are regarded as the major mechanosensors in bone[58] and extend their dendritic processes to communicate with osteoblasts on the bone surface and regulate skeletal anabolic activities by exclusively secreting

sclerostin.[59] Osteocyte expressions of Sost and sclerostin were increased under mechanical unloading, and decreased under enhanced mechanical stimulation.[60] The present study also showed similar findings that expression of Sost mRNA was increased in rat tibias after 4-week HU in both young mature and mature adult rats; nevertheless, PEMF did not exert obvious effects on tibial Sost mRNA expression in HU rats. Thus, our findings suggest that PEMF might stimulate skeletal anabolic activities in HU rats through direct impacts on effector cells on the bone surface (osteoblasts) rather than affecting mechanosensing cells (osteocytes) in bone matrix, at least in terms of Sost expression. Together, our preliminary findings on molecular signaling pathways demonstrate that Wnt/Lrp5/β-catenin signaling might involve in the regulatory behavior of PEMF in bone remodeling. However, these findings need to be further clarified by using gene-targeted knockout mice and in vitro siRNA techniques in our future studies.

In conclusion, the present study demonstrates that PEMF stimulation partially preserves osteoporotic bone mass, microstructure, and strength by promoting skeletal anabolic activities in HU disuse rats, evidenced by serum biochemical, biomechanical, μCT, and histomorphometric results. Moreover, we also reveal that canonical Wnt signaling might be involved in skeletal anabolic effects of PEMF. Our findings enrich our basic knowledge of the osteogenetic activity of PEMF and highlight that PEMF, as a safe and noninvasive method, might become a clinically applicable treatment modality for disuse osteopenia and/or osteoporosis in addition to an alternative countermeasure for bone loss in spaceflight.

Disclosures

All authors state that they have no conflicts of interest.

Acknowledgments

This work was supported by grants from the National Natural Science Foundation of China (No. 51077128 and 31270889) and the Doctoral Thesis Foundation of the Fourth Military Medical University (No. 2012D01).

Authors' roles: DJ, EPL, and JC designed the research. DJ, JC, YW, FJL, and MGJ performed the research. DJ, YW, GHS, XMW, KNX, CT, EPL, WG, and JL analyzed the data. DJ and JC wrote the paper. Revising manuscript content: DJ, JC, YW, and EPL.

References

1. Lau RY, Guo X. A review on current osteoporosis research: with special focus on disuse bone loss. J Osteoporos. 2011;2011:293808.
2. Takata S, Yasui N. Disuse osteoporosis. J Med Invest. 2001;48(3–4):147–56.
3. LeBlanc A, Schneider V, Shackelford L, et al. Bone mineral and lean tissue loss after long duration space flight. J Musculoskelet Neuronal Interact. 2000;1(2):157–60.
4. Lang TF, Leblanc AD, Evans HJ, Lu Y. Adaptation of the proximal femur to skeletal reloading after long-duration spaceflight. J Bone Miner Res. 2006;21(8):1224–30.
5. Riggs BL, Khosla S, Melton LJ 3rd. A unitary model for involutional osteoporosis: estrogen deficiency causes both type I and type II osteoporosis in postmenopausal women and contributes to bone loss in aging men. J Bone Miner Res. 1998;13(5):763–73.
6. Caillot-Augusseau A, Vico L, Heer M, et al. Space flight is associated with rapid decreases of undercarboxylated osteocalcin and increases of markers of bone resorption without changes in their circadian variation: observations in two cosmonauts. Clin Chem. 2000;46(8 Pt 1):1136–43.
7. Lang T, LeBlanc A, Evans H, Lu Y, Genant H, Yu A. Cortical and trabecular bone mineral loss from the spine and hip in long-duration spaceflight. J Bone Miner Res. 2004;19(6):1006–12.
8. Thomsen JS, Morukov BV, Vico L, Alexandre C, Saparin PI, Gowin W. Cancellous bone structure of iliac crest biopsies following 370 days of head-down bed rest. Aviat Space Environ Med. 2005;76(10):915–22.
9. Lazo MG, Shirazi P, Sam M, Giobbie-Hurder A, Blacconiere MJ, Muppidi M. Osteoporosis and risk of fracture in men with spinal cord injury. Spinal Cord. 2001;39(4):208–14.
10. Nelson HD, Humphrey LL, Nygren P, Teutsch SM, Allan JD. Postmenopausal hormone replacement therapy: scientific review. JAMA. 2002;288(7):872–81.
11. Mahavni V, Sood AK. Hormone replacement therapy and cancer risk. Curr Opin Oncol. 2001;13(5):384–9.
12. Paterson CR. Vitamin-D poisoning: survey of causes in 21 patients with hypercalcaemia. Lancet. 1980;1(8179):1164–5.
13. Li K, Kaaks R, Linseisen J, Rohrmann S. Associations of dietary calcium intake and calcium supplementation with myocardial infarction and stroke risk and overall cardiovascular mortality in the Heidelberg cohort of the European Prospective Investigation into Cancer and Nutrition study (EPIC-Heidelberg). Heart. 2012;98(12):920–5.
14. Canalis E, Giustina A, Bilezikian JP. Mechanisms of anabolic therapies for osteoporosis. N Engl J Med. 2007;357(9):905–16.
15. McElhaney JH, Stalnaker R, Bullard R. Electric fields and bone loss of disuse. J Biomech. 1968;1(1):47–52.
16. O'Connor BT, Charlton HM, Currey JD, Kirby DR, Woods C. Effects of electric current on bone in vivo. Nature. 1969;222(5189):162–3.
17. Bassett CA, Pawluk RJ, Pilla AA. Augmentation of bone repair by inductively coupled electromagnetic fields. Science. 1974;184(4136):575–7.
18. Bassett CA, Mitchell SN, Gaston SR, Pulsing electromagnetic field treatment in ununited fractures and failed arthrodeses. JAMA. 1982;247(5):623–8.
19. Assiotis A, Sachinis NP, Chalidis BE. Pulsed electromagnetic fields for the treatment of tibial delayed unions and nonunions. A prospective clinical study and review of the literature. J Orthop Surg Res. 2012;7:24.
20. Ryang We S, Koog YH, Jeong KI, Wi H. Effects of pulsed electromagnetic field on knee osteoarthritis: a systematic review. Rheumatology (Oxford). 2013;52(5):815–24.
21. Thamsborg G, Florescu A, Oturai P, Fallentin E, Tritsaris K, Dissing S. Treatment of knee osteoarthritis with pulsed electromagnetic fields: a randomized, double-blind, placebo-controlled study. Osteoarthritis Cartilage. 2005;13(7):575–81.
22. Kotani H, Kawaguchi H, Shimoaka T, et al. Strong static magnetic field stimulates bone formation to a definite orientation in vitro and in vivo. J Bone Miner Res. 2002;17(10):1814–21.
23. Chang K, Chang WH. Pulsed electromagnetic fields prevent osteoporosis in an ovariectomized female rat model: a prostaglandin E2-associated process. Bioelectromagnetics. 2003;24(3):189–98.
24. Jing D, Cai J, Shen G, et al. The preventive effects of pulsed electromagnetic fields on diabetic bone loss in streptozotocin-treated rats. Osteoporos Int. 2011;22(6):1885–95.
25. Jing D, Shen G, Huang J, et al. Circadian rhythm affects the preventive role of pulsed electromagnetic fields on ovariectomy-induced osteoporosis in rats. Bone. 2010;46(2):487–95.
26. Sert C, Mustafa D, Duz MZ, Aksen F, Kaya A. The preventive effect on bone loss of 50-Hz, 1-mT electromagnetic field in ovariectomized rats. J Bone Miner Metab. 2002;20(6):345–9.
27. Tabrah F, Hoffmeier M, Gilbert F Jr, Batkin S, Bassett CA. Bone density changes in osteoporosis-prone women exposed to pulsed electromagnetic fields (PEMFs). J Bone Miner Res. 1990;5(5):437–42.
28. Eyres KS, Saleh M, Kanis JA. Effect of pulsed electromagnetic fields on bone formation and bone loss during limb lengthening. Bone. 1996;18(6):505–9.
29. Garland DE, Adkins RH, Matsuno NN, Stewart CA. The effect of pulsed electromagnetic fields on osteoporosis at the knee in individuals with spinal cord injury. J Spinal Cord Med. 1999;22(4):239–45.

30. Bodamyali T, Bhatt B, Hughes FJ, et al. Pulsed electromagnetic fields simultaneously induce osteogenesis and upregulate transcription of bone morphogenetic proteins 2 and 4 in rat osteoblasts in vitro. Biochem Biophys Res Commun. 1998;250(2):458–61.
31. Diniz P, Shomura K, Soejima K, Ito G. Effects of pulsed electromagnetic field (PEMF) stimulation on bone tissue like formation are dependent on the maturation stages of the osteoblasts. Bioelectromagnetics. 2002;23(5):398–405.
32. Zhang X, Zhang J, Qu X, Wen J. Effects of different extremely low-frequency electromagnetic fields on osteoblasts. Electromagn Biol Med. 2007;26(3):167–77.
33. Chang K, Chang WH, Huang S, Shih C. Pulsed electromagnetic fields stimulation affects osteoclast formation by modulation of osteoprotegerin, RANK ligand and macrophage colony-stimulating factor. J Orthop Res. 2005;23(6):1308–14.
34. Chang K, Hong-Shong Chang W, Yu YH, Shih C. Pulsed electromagnetic field stimulation of bone marrow cells derived from ovariectomized rats affects osteoclast formation and local factor production. Bioelectromagnetics. 2004;25(2):134–41.
35. Swift JM, Nilsson MI, Hogan HA, Sumner LR, Bloomfield SA. Simulated resistance training during hindlimb unloading abolishes disuse bone loss and maintains muscle strength. J Bone Miner Res. 2010;25 (3):564–74.
36. Halloran BP, Bikle DD, Wronski TJ, Globus RK, Levens MJ, Morey-Holton E. The role of 1,25-dihydroxyvitamin D in the inhibition of bone formation induced by skeletal unloading. Endocrinology. 1986;118(3):948–54.
37. Machwate M, Zerath E, Holy X, et al. Systemic administration of transforming growth factor-beta 2 prevents the impaired bone formation and osteopenia induced by unloading in rats. J Clin Invest. 1995;96(3):1245–53.
38. Morey-Holton ER, Globus RK. Hindlimb unloading rodent model: technical aspects. J Appl Physiol. 2002;92(4):1367–77.
39. Luo E, Shen G, Xie K, et al. Alimentary hyperlipemia of rabbits is affected by exposure to low-intensity pulsed magnetic fields. Bioelectromagnetics. 2007;28(8):608–14.
40. Turner CH, Burr DB. Basic biomechanical measurements of bone: a tutorial. Bone. 1993;14(4):595–608.
41. Bouxsein ML, Boyd SK, Christiansen BA, Guldberg RE, Jepsen KJ, Muller R. Guidelines for assessment of bone microstructure in rodents using micro-computed tomography. J Bone Miner Res. 2010;25(7):1468–86.
42. Ju YI, Sone T, Ohnaru K, Choi HJ, Fukunaga M. Differential effects of jump versus running exercise on trabecular architecture during remobilization after suspension-induced osteopenia in growing rats. J Appl Physiol (1985). 2012;112(5):766–72.
43. Lam H, Qin YX. The effects of frequency-dependent dynamic muscle stimulation on inhibition of trabecular bone loss in a disuse model. Bone. 2008;43(6):1093–100.
44. Wang X, Guo B, Li Q, et al. miR-214 targets ATF4 to inhibit bone formation. Nat Med. 2013;19(1):93–100.
45. Laib A, Kumer JL, Majumdar S, Lane NE. The temporal changes of trabecular architecture in ovariectomized rats assessed by MicroCT. Osteoporos Int. 2001;12(11):936–41.
46. Macias BR, Swift JM, Nilsson MI, Hogan HA, Bouse SD, Bloomfield SA. Simulated resistance training, but not alendronate, increases cortical bone formation and suppresses sclerostin during disuse. J Appl Physiol (1985). 2012;112(5):918–25.
47. Lloyd SA, Bandstra ER, Willey JS, et al. Effect of proton irradiation followed by hindlimb unloading on bone in mature mice: a model of long-duration spaceflight. Bone. 2012;51(4):756–64.
48. Sun LW, Fan YB, Li DY, et al. Evaluation of the mechanical properties of rat bone under simulated microgravity using nanoindentation. Acta Biomater. 2009;5(9):3506–11.
49. Sun Y, Shuang F, Chen DM, Zhou RB. Treatment of hydrogen molecule abates oxidative stress and alleviates bone loss induced by modeled microgravity in rats. Osteoporos Int. 2013; 24(3):969–78.
50. Schriefer JL, Robling AG, Warden SJ, Fournier AJ, Mason JJ, Turner CH. A comparison of mechanical properties derived from multiple skeletal sites in mice. J Biomech. 2005;38(3):467–75.
51. Shahnazari M, Wronski T, Chu V, et al. Early response of bone marrow osteoprogenitors to skeletal unloading and sclerostin antibody. Calcif Tissue Int. 2012;91(1):50–8.
52. Spatz JM, Ellman R, Cloutier AM, et al. Sclerostin antibody inhibits skeletal deterioration due to reduced mechanical loading. J Bone Miner Res. 2013;28(4):865–74.
53. Swift JM, Swift SN, Nilsson MI, Hogan HA, Bouse SD, Bloomfield SA. Cancellous bone formation response to simulated resistance training during disuse is blunted by concurrent alendronate treatment. J Bone Miner Res. 2011;26(9):2140–50.
54. Baron R, Kneissel M. WNT signaling in bone homeostasis and disease: from human mutations to treatments. Nat Med. 2013;19(2):179–92.
55. Krishnan V, Bryant HU, Macdougald OA. Regulation of bone mass by Wnt signaling. J Clin Invest. 2006;116(5):1202–9.
56. Hofbauer LC, Schoppet M. Clinical implications of the osteoprotegerin/RANKL/RANK system for bone and vascular diseases. JAMA. 2004;292(4):490–5.
57. Wada T, Nakashima T, Hiroshi N, Penninger JM. RANKL-RANK signaling in osteoclastogenesis and bone disease. Trends Mol Med. 2006;12(1):17–25.
58. Jing D, Lu XL, Luo E, Sajda P, Leong PL, Guo XE. Spatiotemporal properties of intracellular calcium signaling in osteocytic and osteoblastic cell networks under fluid flow. Bone. 2013;53(2): 531–40.
59. Moriishi T, Fukuyama R, Ito M, et al. Osteocyte network; a negative regulatory system for bone mass augmented by the induction of Rankl in osteoblasts and Sost in osteocytes at unloading. PLoS One. 2012;7(6):e40143.
60. Robling AG, Niziolek PJ, Baldridge LA, et al. Mechanical stimulation of bone in vivo reduces osteocyte expression of Sost/sclerostin. J Biol Chem. 2008;283(9):5866–75.